



Quasi-static crush behavior of hollow microtruss filled with NMF liquid



Yilun Liu^{a,b}, Tobias A. Schaedler^c, Alan J. Jacobsen^c, Weiyi Lu^d, Yu Qiao^d, Xi Chen^{a,b,*}

^a International Center for Applied Mechanics, SV Lab, School of Aerospace, Xi'an Jiaotong University, Xi'an 710049, China

^b Columbia Nanomechanics Research Center, Department of Earth and Environmental Engineering, Columbia University, New York, NY 10027, USA

^c HRL Laboratories LLC, Malibu, CA 90265, USA

^d Department of Structural Engineering, University of California, San Diego, USA

ARTICLE INFO

Article history:

Available online 8 April 2014

Keywords:

Energy absorption
NMF liquid
Microtruss
Plastic buckling
Strain hardening

ABSTRACT

Nanoporous materials functionalized (NMF) liquid has high energy absorption efficiency which holds great promise in advanced protective and damping devices. In this work we incorporate the NMF liquid into hollow microtruss structures to construct a superior energy absorption system. The compressive deformation map of hollow microtruss is given, and then the yielding criterion of NMF liquid filled microtruss is proposed. The quasi-static crush behavior is systematically studied through FEM simulation, then the plastic deformation of the microtruss and NMF liquid are analyzed in detail. By filling NMF liquid into the microtruss the plastic buckling of the microtruss is effectively suppressed, so as to improve the load capacity as well as energy absorption efficiency more than two times for relative thin microtruss ($t/R < 0.02$). The origin of the energy absorption enhancement comes from two parts: one is the volumetric plasticity of NMF liquid and the other part is plastic deformation enhancement of the microtruss. Furthermore, the strain hardening effect of the materials of microtruss can further improve the energy absorption of NMF liquid filled microtruss as the microtruss can hold larger infiltration pressure and reduce the plastic strain localization in the wrinkles of the microtruss to avoid the leaking of NMF liquid.

© 2014 Elsevier Ltd. All rights reserved.

1. Introduction

Developing superior energy absorption materials and structures (EAMS) has been a research focus for both scientists and engineers [2,6,9,22,27]. Cellular structure is perhaps the most widely employed platform of EAMS, thanks to its lightweight and high energy absorption density [11]. The development, design, manufacturing and optimization of cellular structures have been widely studied and reviewed [3,4,30]. Quite many previous works have focused on optimizing the cell geometry, size, topology and materials to improve energy absorption of the cellular structures [10,16,29,31]. Besides energy absorption, cellular structure is also widely employed as building blocks of thermal management [10,26], acoustic isolation [8], catalyst support [4,8] and electrode [4].

Attracted recent attention are the hollow microlattice cellular structures, which have improved mechanical dissipation and heat transfer properties [23]. The enhancement of their efficiency relies on reducing the size of microtruss member, while ensures the

quality of node connection. Recently, Jacobsen et al. [14,15] have developed a new fabrication method based on self-forming photopolymer waveguides that enables both a high degree of control over the geometrical parameters of periodic microlattices and the potential to scale to large areas ($> \text{m}^2$) at high manufacturing throughput (exposure times $\sim 10\text{--}100$ s). This UV photopolymer-based process produces polymeric microlattice cellular materials with a wide range of unit cell sizes (0.1– >10 mm range) and lattice geometries. Subsequent coating of the polymer microlattices, and removal of the polymer result in tube geometries with linear hollow trusses and well-connected nodes [9]. This approach allows for designing the microlattice architecture at three levels of hierarchy: unit cell (symmetry, size, etc.), hollow tube (diameter, wall thickness, node geometry), and hollow-tube wall (micro-structure, composition, multilayer) [24]. Because of the scalability and flexibility of the photopolymer waveguide process, this study focuses on the range of architectures that can be produced using the technique. In particular, hollow microlattice architectures are very attractive for energy absorption and a previous study demonstrated that the hollow tube architecture results in higher energy absorption per weight as compared to foams or solid strut lattice structures [9]. The quasi-static energy absorption characteristics

* Corresponding author at: International Center for Applied Mechanics, SV Lab, School of Aerospace, Xi'an Jiaotong University, Xi'an 710049, China.

E-mail address: xichen@columbia.edu (X. Chen).

of the microlattice structures were investigated experimentally [9] and theoretically [19], which demonstrate promising performance indices. Besides, the very small size of the hollow structure and well connected nodes are very suitable for high efficient heat exchanger [20].

In order to improve the mechanical properties of the cellular structures the cell can be further filled by the elastic filler, such as aluminium foam, polymer foam, liquid and silicon rubber. Previous studies have shown the stiffness, strength and energy absorption of the cellular structures are improved by the additional filler [1,5,7,13,17,30]. In addition, the liquid filler can fit well with cellular structures, avoiding possible problems of filler-network mismatch. However, since most of the liquids are nearly incompressible and therefore cannot accommodate cell compression, the liquid filled cellular structures are often too rigid and easy to rupture during compression; i.e., the major advantage of cellular structures is lost. Recently, a new type of nanoporous materials functionalized (NMF) liquid shows great promise in energy absorption [12,25,33]. For hydrophobic nanoporous materials the liquid molecules can enter the nanopore of the nanoporous materials to generate inelastic volumetric deformation when the applied pressure is larger than a critical value, P_{in} , thus a significant part of the external work is converted to the solid–liquid interfacial energy [18,21], while others are dissipated through the “friction” between infiltrated liquid molecules and solid pore lattice. Here P_{in} is the infiltration pressure of the NMF liquid which is the plateau pressure in the pressure–volume curve shown in Fig. 1(e). Moreover, P_{in} can be precisely tuned by the size of the nanopore and wettability between the liquid and nanopore. The energy absorption

efficiency of NMF liquid is at the level of or above 10–100 J/g, and the volume porosity of the nanopore in NMF liquid is about $n_p = 0.3$ depending on the volume of the nanopore in the nanoporous materials and the volume fraction of nanoporous materials in the NMF liquid [6,12]. Furthermore the response of NMF liquid is very quick, thus it is extremely suitable for mitigating very short time impulse energy and high frequency vibration energy [32]. Therefore, the NMF liquid is a good candidate of pore filler to improve the performance of cellular structures.

In this work we incorporate the highly energy absorbing NMF liquid into hollow microlattice structures to develop a superior energy absorption system. The plastic deformation of NMF liquid filled microtruss is systematically studied through theoretical analysis and FEM simulation. The NMF liquid is filled into the hollow microtruss and sealed by two panels, as schematically shown in Fig. 1(c) and (d). For the predominately 90° microlattice (Fig. 1(a)), based on our previous works [19], the energy absorption is mainly contributed by the large vertical truss. The NMF liquid is fulfilled in the large vertical truss, so in our FEM simulations we use the vertical truss to model the unit cell. By considering the symmetry of 60° microlattice (Fig. 1(b)) the single inclined truss member is employed as unit cell in FEM simulations, and symmetrical boundary conditions are applied to x and z directions as shown in Fig. 1(d). Under compression, the NMF liquid is compatible with the microtruss wall buckling and the infiltration of the NMF liquid can accommodate the compressibility of the NMF liquid filled microtruss. In Section 2, the compressive behavior of both hollow microtruss and NMF liquid filled microtruss is analyzed theoretically and the yielding criterion of NMF liquid filled microtruss is proposed. Thereafter, the finite element method (FEM) simulation of NMF liquid and solid shell is investigated. The quasi-static crush behavior and energy absorption of the NMF liquid filled microtruss are presented in Section 3. In Section 4, the influence of the strain hardening effect of the materials of the microtruss is studied, followed by the discussions of the rupture of the hollow microtruss in Section 5 and conclusions in Section 6.

2. Theoretical benchmarks

In what follows we will first analyze the compressive behavior of hollow microtruss and construct a map of buckling modes for different geometrical parameters of the hollow microtruss. Then, the compressive behavior of NMF liquid filled microtruss is discussed and a yielding criterion is deduced.

2.1. Buckling modes of hollow microtruss

During compression of the hollow microtruss, there are three types of buckling modes: the Euler beam buckling, shell buckling, and plastic yielding which depend on the geometrical parameters (length, radius and thickness) and mechanical properties of the parent materials. Based on the classic elastic stability textbook [28], the critical buckling stress $\sigma_{cr,b}$ of Euler beam buckling is

$$\sigma_{cr,b} = E \frac{\pi^2 I}{A(\mu l)^2}, \quad (1)$$

where E is the Young's modulus of the parent materials, A is cross section area, I is bending moment, l is length of the hollow microtruss, μ is the coefficient of effective length which is $\mu = 0.5$ for two ends clamped beam. For the circular hollow truss the cross section area equals to $A = 2\pi R t$, where R is radius of the middle plane of the hollow microtruss and t is thickness, while the bending moment is

$$I = \frac{\pi}{4} [(R + t/2)^4 - (R - t/2)^4] = \frac{A}{2} \left(R^2 + \frac{t^2}{4} \right). \quad (2)$$

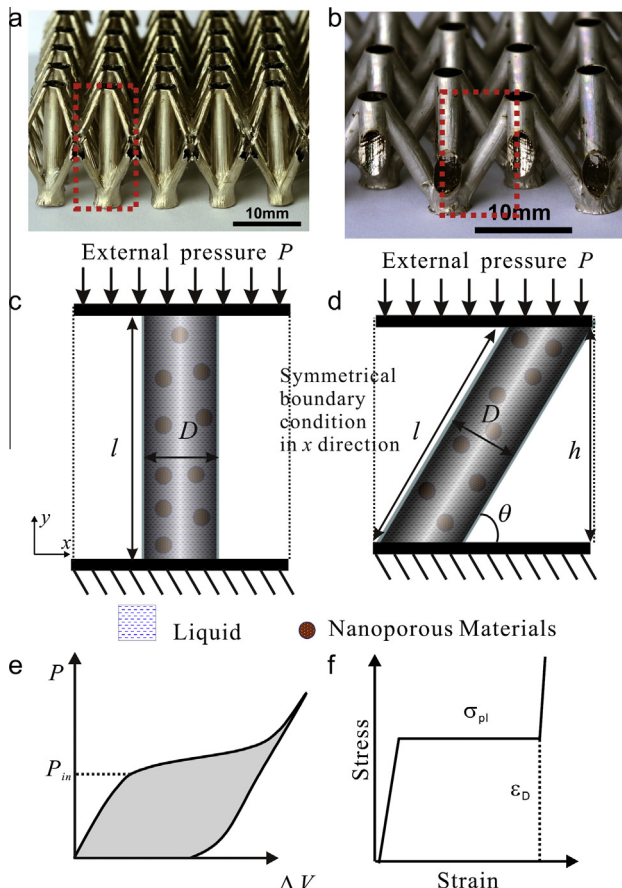


Fig. 1. The representative 90° (a) and 60° (b) hollow microlattice structures in experiment. (c) and (d) The corresponding schematic diagram of FEM simulation model for the microlattice structures with NMF liquid filler. (e) The typical mechanical response of NMF liquid and (d) the ideal mechanical response of EAMS.

Substituting Eq. (2) into Eq. (1) then we get the critical buckling stress is

$$\sigma_{cr,b} = E \frac{\pi^2}{(\mu l)^2} \left(R^2 + \frac{t^2}{4} \right) = E \frac{\pi^2}{\mu^2} \left(\frac{R}{l} \right)^2 \left[1 + \frac{1}{4} \left(\frac{t}{R} \right)^2 \right]. \quad (3)$$

However, in order to obtain Euler beam buckling, the critical stress must be smaller than the yielding stress of the parent materials $\sigma_{cr,b} < \sigma_Y$, so we get the criterion of Euler beam buckling and plastic yielding as

$$\frac{l}{R} = \frac{\pi}{\mu} \sqrt{\frac{E}{\sigma_Y} \left[1 + \frac{1}{4} \left(\frac{t}{R} \right)^2 \right]}. \quad (4)$$

If the ratio of thickness to radius is small, Eq. (4) is simplified to

$$\frac{l}{R} = \frac{\pi}{\mu} \sqrt{\frac{E}{\sigma_Y}}. \quad (5)$$

For the cylindrical shell under uniform axial pressure the critical buckling stress is

$$\sigma_{cr,s} = \frac{E}{\sqrt{3(1-\nu^2)}} \frac{t}{R}, \quad (6)$$

where ν is Poisson ratio of the parent materials. The same as the Euler beam buckling the critical stress must be also smaller than the yield stress of the parent materials $\sigma_{cr,s} < \sigma_Y$ to obtain the shell buckling, so the criterion for shell buckling and plastic yielding is

$$\frac{R}{t} = \frac{E}{\sigma_Y \sqrt{3(1-\nu^2)}}. \quad (7)$$

From Eq. (7) it seems the criterion is independent of l/R . However, Eq. (6) is only valid for long cylindrical shell. For short cylindrical shell, if [28]

$$\left(\frac{l}{\pi R} \right)^2 < \frac{t}{2R\sqrt{3(1-\nu^2)}}, \quad (8)$$

then, the critical shell buckling stress is [28]

$$\sigma_{cr,s} = \frac{\pi^2 E}{12(1-\nu^2)} \frac{t^2}{l^2} = \frac{\pi^2 E}{12(1-\nu^2)} \left(\frac{t}{R} \right)^2 \left(\frac{R}{l} \right)^2. \quad (9)$$

In order to get the elastic buckling $\sigma_{cr,s}$ should be smaller than σ_Y . Therefore, for short cylindrical shell the criterion of plastic yielding and elastic buckling is

$$\frac{l}{R} = \sqrt{\frac{\pi^2 E}{12(1-\nu^2)} \frac{t}{\sigma_Y}}. \quad (10)$$

While the criterion for the Euler beam buckling and shell buckling is the critical buckling stress of beam equals to the critical buckling stress of shell, $\sigma_{cr,b} = \sigma_{cr,s}$, then we get

$$\left(\frac{l}{R} \right)^2 = \frac{\pi^2 \sqrt{3(1-\nu^2)}}{\mu^2} \left(\frac{R}{t} \right) \left[1 + \frac{1}{4} \left(\frac{t}{R} \right)^2 \right]. \quad (11)$$

Based on the previous analysis we obtain the map of compressive buckling modes of hollow microtruss for different geometrical parameters of l/R and R/t which are shown in Fig. 2.

The typical size of the hollow truss microlattice in the experiments is $l = 15$ mm, $R = 1.7$ mm and $t = 0.07$ mm, and the parent material is electroplate nickel with the Young's modulus $E = 200$ GPa, Poisson ratio $\nu = 0.31$ and yielding strength $\sigma_Y = 300$ MPa. Substituting the geometrical and mechanical parameters into Eqs. (4) and (7), it can be deduced that l/R and R/t are much smaller than the criterion of Euler beam buckling and shell buckling, so during compression the deformation of hollow truss

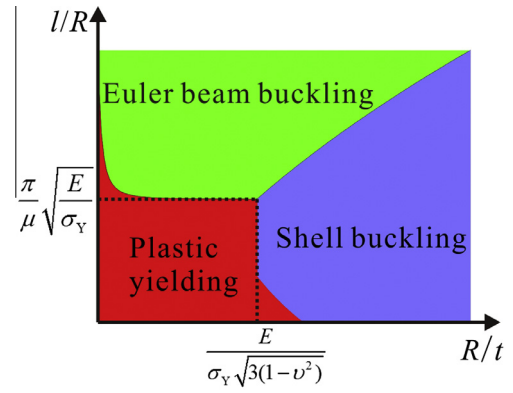


Fig. 2. The compressive buckling modes of hollow microtruss with different geometrical parameters of l/R and R/t .

microlattice is plastic hinges and wrinkles generated by plastic yielding as demonstrated in our previous works [19].

2.2. Yielding criterion of NMF liquid filled microtruss

Based on the aforementioned analysis, the influence of NMF liquid filler to the plastic yielding behavior of hollow microtruss is now investigated. Here, we only consider the quasi-static axial compressive deformation of the NMF liquid filled microtruss. Before plastic yielding, the deformation in the hollow microtruss can be assumed as homogenous.

The parent materials of the hollow microtruss are treated as isotropic elastic-perfectly plastic materials, whose stress–strain relationship before yielding is

$$\begin{aligned} \varepsilon_z &= \frac{1}{E_t} [\sigma_z - \nu_t(\sigma_r + \sigma_\theta)] \\ \varepsilon_\theta &= \frac{1}{E_t} [\sigma_\theta - \nu_t(\sigma_r + \sigma_z)] \\ \varepsilon_r &= \frac{1}{E_t} [\sigma_r - \nu_t(\sigma_z + \sigma_\theta)] \end{aligned} \quad (12)$$

where ε_z and σ_z are strain and stress in the axial direction of the hollow truss, ε_θ and σ_θ are in the circumferential direction, ε_r and σ_r are in the radial direction, E_t is Young's modulus and ν_t is Poisson ratio of the parent materials. As the radial stress σ_r is much smaller than the axial σ_z and circumferential stress σ_θ , in the following analysis we neglect the influence of radial stress to the axial and circumferential strain of the hollow truss. The pressure, P_L , in NMF liquid is

$$P_L = \begin{cases} -K_L \varepsilon_V & (\varepsilon_V > -\frac{P_{in}}{K_L}) \\ P_{in} & (\varepsilon_V \leq -\frac{P_{in}}{K_L}) \end{cases}, \quad (13)$$

where K_L is the bulk modulus of NMF liquid and in the present paper it is dominated by water, so that $K_L = 2$ GPa, ε_V is volumetric strain of NMF liquid. Here the constitutive relation of NMF liquid is assumed as elastic-perfectly plastic where the relation between the pressure and the volumetric deformation is linear when the pressure is smaller than the infiltration pressure P_{in} , otherwise the pressure is constant P_{in} . Here we assume the NMF liquid is fulfilled in the cylindrical shell, so the volumetric strain ε_V is

$$\varepsilon_V = \varepsilon_z + 2\varepsilon_\theta. \quad (14)$$

According to the force equilibrium

$$\frac{\sigma_\theta t}{R} = P_L. \quad (15)$$

Solving Eqs. (12)–(15) we get the axial stress σ_z in the hollow truss expressed by ε_z

$$\sigma_z = \begin{cases} \frac{E_t \varepsilon_z}{1 - \nu_t^2} \left(1 - \frac{k_2 + k_1 \nu_t}{2k_2 + k_1} \nu_t \right) & (\varepsilon_V > -\frac{P_{in}}{K_L}) \\ E_t \varepsilon_z + \frac{P_{in}}{k_1} \nu_t & (\varepsilon_V \leq -\frac{P_{in}}{K_L}) \end{cases}, \quad (16)$$

and the circumferential stress σ_θ in the hollow truss expressed by ε_z

$$\sigma_\theta = \begin{cases} \frac{E_t \varepsilon_z}{1 - \nu_t^2} \frac{k_2(2\nu_t - 1)}{2k_2 + k_1} & (\varepsilon_V > -\frac{P_{in}}{K_L}) \\ \frac{P_{in}}{k_1} & (\varepsilon_V \leq -\frac{P_{in}}{K_L}) \end{cases}, \quad (17)$$

where $k_1 = t/R$, $k_2 = \frac{K_L}{E_t/(1 - \nu_t^2)}$ and the volume strain ε_V is

$$\varepsilon_V = \begin{cases} \frac{k_1(1 - 2\nu_t)}{2k_2 + k_1} \varepsilon_z & (\varepsilon_V > -\frac{P_{in}}{K_L}) \\ \frac{2P_{in}}{k_1 E_t/(1 - \nu_t^2)} + (1 - 2\nu_t) \varepsilon_z & (\varepsilon_V \leq -\frac{P_{in}}{K_L}) \end{cases}. \quad (18)$$

Here ε_z equals to the nominal compressive strain applied to the microtruss. For the NMF liquid filled microtruss there are two types of permanent deformation: the plastic yielding of the hollow microtruss $\sigma_{VM} = \sigma_Y$ and the infiltration of NMF liquid ($\sigma_\theta = P_{in}/k_1$), where σ_{VM} is the Von-Mises stress in the microtruss defined as

$$\sigma_{VM} = \sqrt{\frac{(\sigma_z - \sigma_\theta)^2 + \sigma_z^2 + \sigma_\theta^2}{2}}. \quad (19)$$

Before plastic yielding of the microtruss, the deformation is homogenous and there is no shear deformation in the microtruss. Then the yielding criterion of NMF liquid filled microtruss is

$$\begin{cases} \left| \frac{E_t \varepsilon_z}{1 - \nu_t^2} \sqrt{\frac{\left(1 - \frac{3k_2 \nu_t - k_2 + k_1 \nu_t^2}{2k_2 + k_1}\right)^2 + \left(1 - \frac{k_2 + k_1 \nu_t}{2k_2 + k_1} \nu_t\right)^2 + \left[\frac{k_2(2\nu_t - 1)}{2k_2 + k_1}\right]^2}}{2} \right| = \sigma_Y & (\varepsilon_V^* > -\frac{P_{in}}{K_L}) \\ \frac{E_t \varepsilon_z}{1 - \nu_t^2} \frac{k_2(2\nu_t - 1)}{2k_2 + k_1} = \frac{P_{in}}{k_1} & (\varepsilon_V^* \leq -\frac{P_{in}}{K_L}) \end{cases}. \quad (20)$$

Here ε_V^* is the volumetric strain at the yielding point of microtruss which is

$$\varepsilon_V^* = -\frac{k_1(1 - 2\nu_t)}{2k_2 + k_1} \frac{\sigma_Y}{\frac{E_t}{1 - \nu_t^2} \sqrt{\frac{\left(1 - \frac{3k_2 \nu_t - k_2 + k_1 \nu_t^2}{2k_2 + k_1}\right)^2 + \left(1 - \frac{k_2 + k_1 \nu_t}{2k_2 + k_1} \nu_t\right)^2 + \left[\frac{k_2(2\nu_t - 1)}{2k_2 + k_1}\right]^2}}}. \quad (21)$$

For the studied NMF liquid filled microlattice structures in the experiments, the yielding strength of the microtruss is $\sigma_Y = 300$ MPa and the infiltration pressure of the NMF liquid is about several tens of MPa. For the range of parameters studied herein, the microtruss material yields first. After yielding, wrinkles and plastic hinges occur in the microtruss, so that the compressive deformation is no longer homogenous. With continued compression, the pressure of the filled NMF liquid reaches infiltration pressure P_{in} and triggers NMF liquid infiltration, the second permanent deformation mechanism. In the following section, FEM models are employed to simulate the post plastic buckling behavior and energy absorption characteristics of NMF liquid filled microtruss.

3. FEM simulations

In what following we first build the FEM simulation model for the NMF liquid which can describe its fluidic and infiltration behavior. Then, the quasi-static crush behavior and energy absorption characteristics of NMF liquid filled microtruss are systematically studied for different geometrical parameters and inclined

angles of the microtruss. The plastic deformation of the microtruss and inelastic deformation of NMF liquid is analyzed in detail. Thereafter, comparison to the experiments is given.

3.1. Simulation model

The representative unit cells of NMF liquid filled microtruss for predominately 90° and 60° microlattice structures are schematically shown in Fig. 1(c) and (d). The hollow microtruss is fully filled by NMF liquid and sealed by two flat panels. The parent material of the microtruss is electroplated nickel, with density $\rho_s = 8.9$ g/cc, Young's modulus $E = 200$ GPa, and yield strength $\sigma_Y = 300$ MPa [9]. The strain hardening effect of nickel is very weak, so the stress-strain behavior of nickel is assumed elastic-perfectly plastic in Section 3. The effect of strain hardening to the compressive deformation and energy absorption of NMF filled microtruss is given separately in Section 4. We further ignore any fracture process that may occur during the compression in the FEM simulation (the rupture of the microtruss and its influence on the leaking of NMF liquid filler are discussed in Section 5). In current work, all the experiments and simulations are under quasi-static loading condition.

The NMF liquid is formed by dispersing lyophobic nanoporous materials into liquid. The typical compressive behavior of NMF liquid has three stages: the elastic deformation of the liquid and the void nanoporous material, the infiltration of the liquid molecules into the nanoporous material (inelastic volumetric deformation) when the applied pressure is larger than the capillary pressure of the nanopore P_{in} , and the densification after all of the nanopores are filled by the liquid, Fig. 1(e) [33]. In order to phenomenologically describe the compressive behavior of NMF liquid, the equation of state (EOS) method in ABAQUS is used. The elastic deformation of the NMF liquid is described by a linear $U_s - U_p$ Hugoniot form combining with the $P - \alpha$ EOS compaction to describe the inelastic volumetric deformation of the infiltration process. The relationship between pressure P and density ρ of NMF liquid is

$$P = \frac{\rho_0 c_0^2 \eta}{(1 - s\eta)^2} \left(1 - \frac{\Gamma_0 \eta}{2} \right) + \Gamma_0 \rho_0 E_m \quad (22)$$

where ρ_0 is the reference density and ρ is the density of the NMF liquid during compression, η is defined as $\eta = 1 - \rho_0/\rho$, $\rho_0 c_0^2$ is equivalent to the bulk modulus at small strain, and E_m is internal energy. In the present study, $\rho_0 = 1000$ kg/m³, $c_0 = 1414$ m/s, so that $\rho_0 c_0^2 = 2$ GPa equals to the bulk modulus of water, and we further simplify $s = 0$ and $\Gamma_0 = 0$. In order to describe the infiltration effect, we use $P - \alpha$ equation of state where the pressure depends on the density ρ and the minimum value of the state variable α_{min} ($\alpha = \frac{\rho_0}{\rho}$) during loading. The EOS model can describe the volumetric strength and infiltration of the NMF liquid, but does not account for the macroscopic flow viscosity of NMF liquid (which is reflected in part through the phenomenological infiltration pressure). However, for the present problem where the NMF liquid is confined in the microtruss, the macroscopic flow of NMF liquid is small and the flow viscosity has little influence to the energy absorption.

Before studying the energy absorption of NMF liquid filled microtruss, we first simulate a simple system of circular nickel pad filled by NMF liquid to verify the computational model, shown in Fig. 3(a). The radius of the nickel shell is 14 mm, height is 4.4 mm and thickness is 0.05 mm. The general purpose shell element S4R is employed to describe the nickel shell, and the NMF liquid is described via C3D8R element by EOS method throughout the paper, and a mesh convergence study is carried out. As the radius of the circular shell is much larger than its height, buckling of the nickel

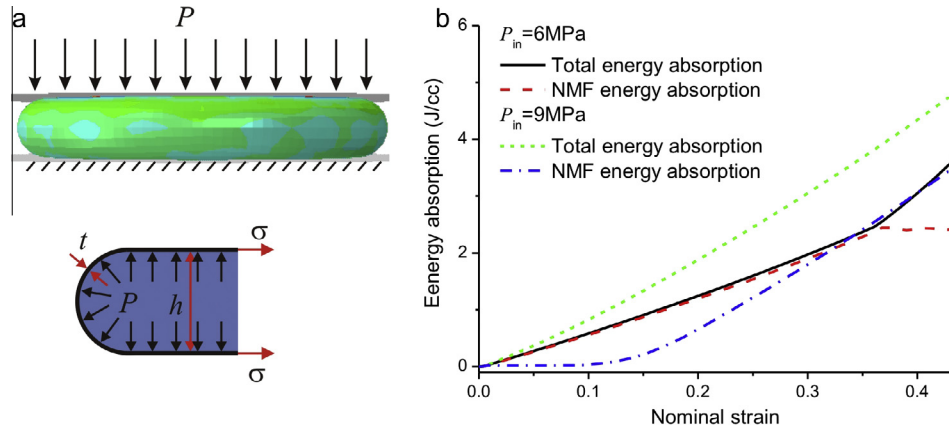


Fig. 3. Energy absorption of NMF liquid and nickel shell. (a) The schematic illustration of the NMF liquid and nickel shell model in the simulation. (b) The energy absorption of the NMF liquid and whole system for different infiltration pressures $P_{in} = 6$ MPa and $P_{in} = 9$ MPa.

shell is prohibited during compression. This is suitable to analyze the energy absorption mechanism of NMF liquid filled system. Two different infiltration pressures, $P_{in} = 6$ MPa and $P_{in} = 9$ MPa with the same porosity $n_p = 0.3$, are simulated to study the influence of the infiltration pressure of the NMF liquid to the energy absorption of the hybrid system.

The energy absorbed by the whole system and the NMF liquid are tracked during compression. For the infiltration pressure of $P_{in} = 6$ MPa, the energy absorption is contributed by the NMF liquid when the nominal strain is smaller than 0.35. After that, the energy absorption is contributed by the plastic deformation of the nickel shell and the energy absorption of the NMF liquid is saturated. However, for the infiltration pressure $P_{in} = 9$ MPa, the external energy is dissipated firstly by the plastic deformation of nickel shell when the nominal strain is smaller than 0.15, after that the extra energy is absorbed by the NMF liquid.

By considering the force equilibrium in the nickel shell, the pressure of NMF liquid acting on the circumferential shell should be equilibrated by the stress σ

$$\sigma = P \frac{h}{2t}. \tag{23}$$

Since the radial stress cannot be larger than the yield strength, $\sigma \leq \sigma_y$, which determines the maximum value of the infiltration pressure P_{in} in the NMF liquid as

$$P_{in} = \sigma_y \frac{2t}{h}. \tag{24}$$

For the above simulated system, the maximum infiltration is $P_{in} = 6.8$ MPa. Therefore, for the NMF liquid with $P_{in} = 9$ MPa, the infiltration does not occur at small deformation. As the compression proceeds, the height h of the nickel shell decreases so as to increase the maximum attainable pressure, and finally induces infiltration. Next, we examine the compressive behavior and energy absorption characteristics of the NMF liquid and microtruss system.

The NMF liquid can accommodate well with the wall buckling of the microtruss which makes it an ideal pore filler to improve the energy absorption of the microtruss system. Due to the very large specific surface area of the nanoporous materials, the hybrid system of NMF liquid and microtruss system holds great promise in energy absorption [6]. The quasi-static crush behavior of the microtruss filled with NMF liquid is simulated by FEM. With reference to Fig. 1(c) and (d), the hollow microtruss unit cell is filled with NMF liquid and sealed by two plates. The NMF liquid is tied to the inner surface of the microtruss and the general contact procedure is employed to describe the self-contact of microtruss and

contact between the microtruss and top and bottom plates. The bottom plate is fixed and the top plate is compressed vertically towards to the bottom plate at a given velocity. The reaction force acting on the top plate is tracked during compression and then the energy absorption is deduced.

3.2. Compressive behavior

The compressive deformation of 60° microtruss with NMF liquid and without NMF liquid is shown in Fig. 4. The wall thickness of the microtruss is $t = 0.07$ mm, radius $R = 1.7$ mm and length $l = 15$ mm. The infiltration pressure of the NMF liquid is an important parameter for the energy absorption of NMF liquid filled microtruss. Here for the studied microtruss we set $P_{in} = 9$ MPa (which is the optimized infiltration pressure for the given microtruss; more discussions on the optimized pressure for NMF liquid-microtruss system will be elaborated in Section 3.3). The porosity of the NMF liquid is $n_p = 0.3$, which is consistent with the previous experiment [6]. For the 60° hollow microtruss wrinkles are localized near the ends after initial yield, leading to plastic “hinges”. Subsequently, the system “crushing” (Fig. 4(b)) and the load capacity quickly reduces, followed by a long plateau before densification (see the dashed line in Fig. 6). However, if the microtruss is filled by NMF liquid, the plastic “hinges” are effectively

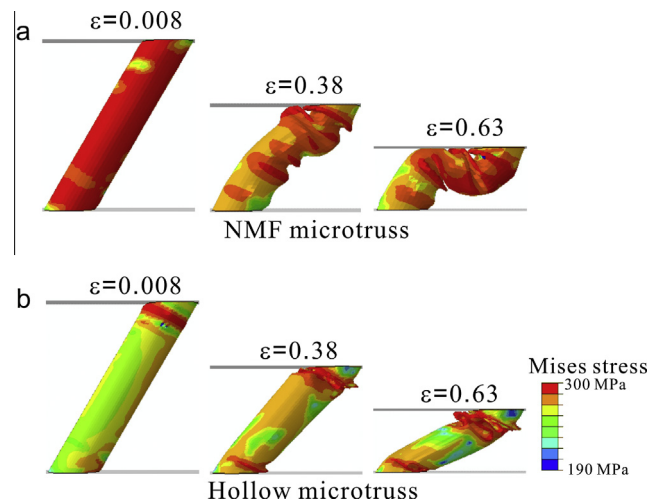


Fig. 4. The compressive deformation of 60° microtruss unit cell with NMF liquid (a) and without NMF liquid (b) at different nominal compressive strain. $t = 0.07$ mm, $R = 1.7$ mm and $l = 15$ mm.

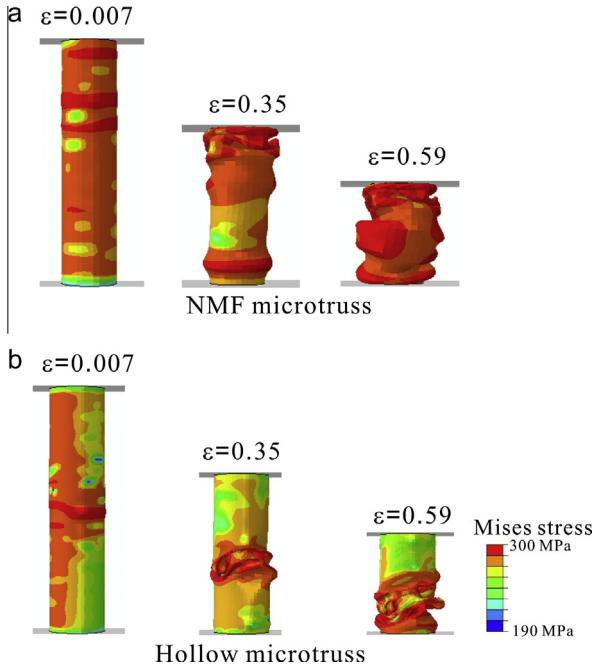


Fig. 5. The compression deformation of 90° microtruss with NMF liquid (a) and without NMF liquid (b) at different nominal compressive strain with the wall thickness of the microtruss $t = 0.07$ mm, radius $R = 1.7$ mm and length $l = 15$ mm.

suppressed, therefore the sudden “crushing” is avoided. Owing to the support of NMF liquid to the wall of the microtruss, the overall deformation is beam-like bending and the wave length of the wrinkles is also larger. Besides, the stress distribution in the microtruss with NMF liquid filler is more uniform than the hollow microtruss, see the contour plots in Fig. 4. Thus more energy can be dissipated by the shell of the microtruss. Here the contour plots in Fig. 4 represent the von Mises stress distribution in the microtruss and the legend is shown in the lower right corner. The post buckling load capacity of NMF liquid filled microtruss is larger than the value of hollow microtruss (see the solid line in Fig. 6) and is approaching the ideal response of EAMS in Fig. 1(e).

To illustrate the influence of inclination angle, the comparison of 90° microtruss with NMF liquid and without NMF liquid is also studied with the same wall thickness, radius and length. The optimized infiltration pressure is 10 MPa and the porosity of the NMF liquid is $n_p = 0.3$. For the 90° hollow microtruss, the wrinkles are generated at the middle region of the microtruss after initial buckling and the wrinkles propagate to both ends with compression proceeding. For NMF liquid filled 90° microtruss, there are also some long-wavelength wrinkles generated after initial buckling, and the stress distribution is more uniform than the case of hollow microtruss, see the contour plots Fig. 5. The post buckling load capacity is larger than the value of hollow microtruss, therefore the energy absorption is enhanced.

The history of compressive pressure, P , acting on the top panel as shown in Fig. 1(c) and (d) is analyzed. The non-dimensional nominal stress in the microtruss is defined as $P/\bar{\rho}\sigma_y$, where $\bar{\rho}$ is relative density of hollow microlattice. For 60° microlattice, it equals to [9]

$$\bar{\rho} = \frac{32\pi Rt}{\sqrt{3}l^2} = \frac{32\pi}{\sqrt{3}} \left(\frac{R}{l}\right)^2 \frac{t}{R}. \quad (25)$$

The initial buckling stress of microtruss with NMF liquid filler and without NMF liquid filler is almost the same for both 60° microtruss and 90° microtruss, respectively. The non-dimensional

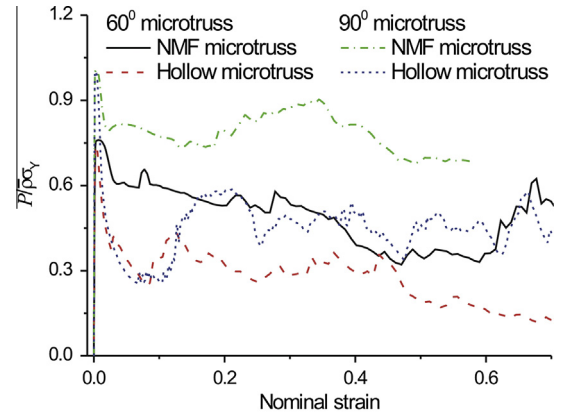


Fig. 6. The non-dimensional stress and nominal strain curves for the microtruss with and without NMF liquid for the compressive deformation shown in Figs. 4 and 5.

initial buckling stress for 60° microtruss is about 0.75 and for 90° microtruss is about 1 which is consistent with the previous results for hollow microtruss [19]. As the bulk modulus of NMF liquid is much smaller than the Young’s modulus of nickel, the contribution to the initial buckling stress by the NMF liquid is very small. This is consistent with our theoretical analysis in Section 2. However, after the initial buckling, in contrast to the rapid decreasing of the load capacity for hollow microtruss, the weakening of load capacity for NMF liquid filled microtruss is smaller, especially for 90° microtruss, see Fig. 6. The energy absorption of NMF liquid filled microtruss is improved by about 80% for the given parameters. The influence of the geometrical parameters of the microtruss to the energy enhancement will be discussed later. During compression, the initial buckling stress is the peak stress σ_p (for both 60° and 90° microtruss with and without NMF liquid). In practical application, the peak stress should be smaller than damage threshold stress σ_{th} ($\sigma_p \leq \sigma_{th}$) of the protected devices. The NMF liquid filler can increase the energy absorption but does not increase the peak stress which is particular desired in protective structures.

3.3. Energy absorption enhancement

The infiltration pressure of NMF liquid is very important to the energy absorption of NMF liquid filled microtruss. The maximum absorbed energy per volume of the NMF liquid is on the order of $P_{in}n_p$. According to previous experiment, the porosity n_p of the NMF liquid is about 0.3 and is difficult to improve further [6]. In order to fulfill the energy absorption capability of NMF liquid, the infiltration pressure should be as large as possible. However, if the infiltration pressure is too large, the infiltration process cannot occur and it is also limited by the damage threshold of the protected device; moreover, the compressibility of the NMF liquid filled microtruss is weakened and the microtruss may be ruptured during compression. The maximum infiltration pressure is constrained by the geometry of the surrounding structures and yield strength of the surrounding materials, as discussed in Section 3.1. For microtruss, based on the force equilibrium the maximum infiltration pressure is bounded by $\sigma_y t/R$. For the microtruss with thickness $t = 0.07$ mm, radius $R = 1.7$ mm and the yield strength of parent material 300 MPa, the maximum infiltration pressure constrained by the structure and material is 12.4 MPa. However, the maximum infiltration pressure cannot be always sustained by the microtruss because of the very complicated deformation of the microtruss during compression. Here the optimized infiltration pressure is selected to maximize the energy absorption of NMF liquid during compression. For 60° microtruss the optimized

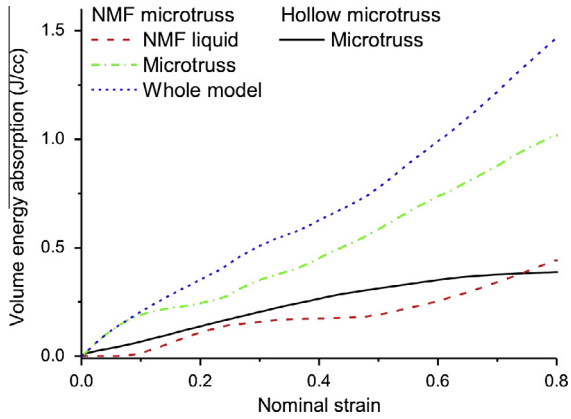


Fig. 7. The comparison of the energy absorption of hollow microtruss and NMF liquid filled microtruss during compression for 60° microtruss with the wall thickness of the microtruss $t = 0.02$ mm, radius $R = 1.7$ mm and length $l = 20$ mm.

infiltration pressure is 9 MPa and for 90° microtruss it is 10 MPa (with the given material and geometrical parameters). This is different from the simple structures simulated in Fig. 3 where the nickel shell can hold the maximum infiltration pressure. For microtruss, as the global bending and local wrinkles are accompanied with compression, after the global bending or local wrinkles occurred, the pressure in the NMF liquid is released so the maximum infiltration pressure may not be kept. According to the FEM simulation, the optimized infiltration pressure for 60° microtruss is about $0.7\sigma_Y t/R$ and for 90° microtruss is about $0.8\sigma_Y t/R$, for different geometrical parameters t/R from 0.01 to 0.09 and R/l from 0.085 to 0.17.

From Fig. 6, the load capacity is increased by filling NMF liquid into the microtruss, so energy absorption is improved. The energy absorption enhancement comes from two parts, the additional energy absorption by volumetric inelastic deformation of NMF liquid and the energy absorption enhancement by microtruss. For example, the energy absorption by NMF liquid and microtruss for the 60° microtruss with the wall thickness $t = 0.02$ mm, radius $R = 1.7$ mm and length $l = 20$ mm are given in Fig. 7. For an NMF liquid filled microtruss, as the supporting of NMF liquid the plastic buckling of microtruss shell is highly suppressed and the plastic deformation in the microtruss is more uniform so as to double the energy absorption of the shell, see the green dash dotted line and black line Fig. 7. In addition, the NMF liquid will provide another fold, see the red dashed line¹ in Fig. 7, so that the total energy absorption of NMF filled microtruss is 3.3 folds of value of the hollow microtruss.

The effect of geometrical parameters is illustrated next. The total energy enhancement of the NMF liquid filled microtruss for 90° and 60° microtruss with t/R from 0.01 to 0.09 and R/l from 0.085 to 0.17 is given in Fig. 8. As t/R increases, the ratio of the energy absorption between NMF liquid filled microtruss and hollow microtruss $E_{\text{NMFtruss}}/E_{\text{Hollow}}$ decreases from 3 ($t/R = 0.01$) to 1.5 ($t/R = 0.09$). This is because the mass ratio between NMF liquid to the hollow microtruss is inversely proportional to t/R , and for smaller t/R the enhancement by NMF liquid filler is larger. The influence of R/l and inclined angle of the microtruss to the energy absorption enhancement is small.

The transmitted stress, σ_{tr} , is an important parameter for EAMS. In practical application, the maximum transmitted stress should be smaller than the damage threshold stress of the protected devices

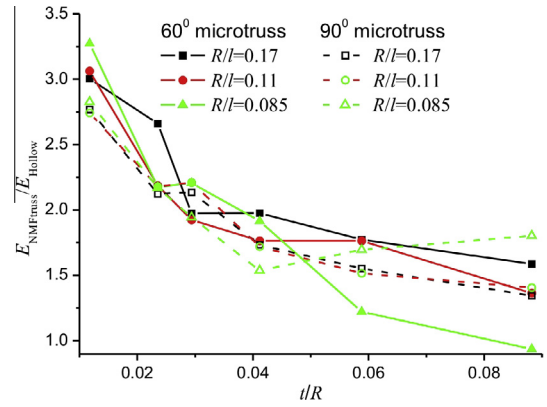


Fig. 8. The energy absorption enhancement of NMF liquid filled microtruss to hollow microtruss for 90° microtruss with different $R/l = 0.17$ (open squares), $R/l = 0.11$ (open circles), $R/l = 0.085$ (open triangles) and 60° microtruss with different $R/l = 0.17$ (solid squares), $R/l = 0.11$ (solid circles), $R/l = 0.085$ (solid triangles).

($\sigma_{\text{tr}} \leq \sigma_{\text{th}}$). Therefore, the maximum energy absorption per volume is bounded by the damage threshold stress as

$$E_{\text{max}} = \sigma_{\text{th}} \left(1 - \frac{\sigma_{\text{th}}}{\sigma_Y} \right), \quad (26)$$

where $(1 - \sigma_{\text{th}}/\sigma_Y)$ is the upper bound densification strain of EAMS. If the EAMS has an ideal mechanical response like that shown in Fig. 1(f), with the plateau stress σ_{pl} equals to the damage threshold stress σ_{th} , and the EAMS is completely compressed to densification, the upper bound energy absorption can be achieved. For hollow truss microlattice structures, the densification strain is usually about 0.85 which is slightly smaller than $(1 - \sigma_{\text{th}}/\sigma_Y)$ (~ 0.98). However, for the hollow microtruss structures, the maximum transmitted stress usually occurs at the initial buckling of the microtruss which is larger than the plateau stress, see Fig. 6. Therefore, the upper bound energy absorption is hard to achieve. The relationship between volume energy absorption density and damage threshold stress for NMF liquid filled microtruss and hollow microtruss is given in Fig. 9. The volume energy absorption density is well bounded by Eq. (26). The NMF liquid filler does not increase the maximum transmitted stress of microtruss system, but increases plateau stress, so it is more approaching to the upper bound line.

3.4. Comparison with experiments

In order to validate the simulations, a model system of NMF liquid filled microlattice was investigated experimentally. Quasi-static crush tests were conducted on 60° hollow and NMF liquid filled microlattice structures with the wall thickness $t = 0.03$ mm, radius $R = 1.7$ mm and length $l = 15$ mm, with relative density about 1.2%. The as-received nanoporous silica particles were modified by trimethylchlorosilane (TMCS) to convert the naturally lyophilic surface to lyophobic. The details of the surface modification have been reported elsewhere [12,25,33]. Then, the pretreated silica particles were dispersed into the liquid phase of 20wt 1-Butyl-3-methylimidazolium tetrafluoroborate (BMIMBF₄) aqueous solution. Upon external loading the NMF liquid exhibited an infiltration stage from 0.8 MPa to 3 MPa, as shown in Fig. 10 the sorption isotherm curve of the NMF liquid which is consistent with the FEM simulation model. Here, because the nanopores in the silica particles were not uniform, the infiltration pressure was not a constant since the largest nanopore was firstly filled by liquid.

In order to fill the NMF liquid into the hollow microlattice structures, a stainless steel plate was attached to one end of the microlattice by an Ecotech underwater adhesive. Then, the NMF

¹ For interpretation of color in Fig. 7, the reader is referred to the web version of this article.

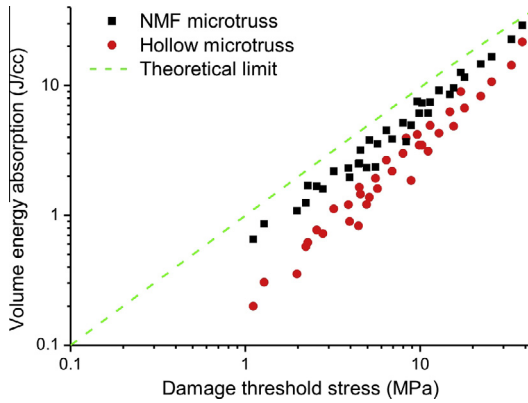


Fig. 9. The relation between energy absorption per volume and damage threshold stress for NMF filled microtruss (squares) and hollow microtruss (circles). The dashed line is the upper limit of volume energy absorption density.

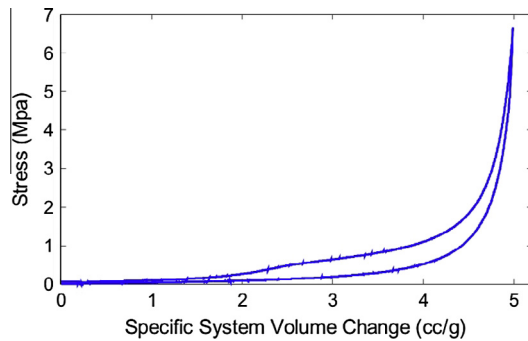


Fig. 10. Sorption isotherm curve of selected NMF liquid filler.

liquid was injected into the hollow microtruss and the filled microlattice was sealed by another stainless steel plate using the same adhesive. Here, for the comparison the hollow microlattice structures were also attached by two stainless steel plates; see also Fig. 11(a) and (b). Afterward the hollow and NMF liquid filled

microlattice structures were compressed by an Instron machine quasi-statically, and the compressive deformation was illustrated in Fig. 11(a) and (b). Similar to the FEM simulation results, there are wrinkles and plastic “hinges” generated in the hollow microlattice, while for the NMF filled microlattice the wrinkles are effectively suppressed and the deformation is more permanent.

The compressive stress–strain curves of both systems (Fig. 11) are given in Fig. 12. The post buckling stress of the NMF liquid filled microlattice is almost identical to the initial buckling stress, so that the mechanical response of NMF liquid filled microlattice approaches the ideal mechanical response of EAMS shown in Fig. 1(d), while for the hollow microlattice the load capacity is significantly weakened after the initial buckling which is consistent with the previous FEM simulation results. Here the peak stress (the initial yielding stress) of the empty structure and NMF liquid filled structure is different, as given in Fig. 12. This is because the peak stress is usually influenced by defects of the microlattice structure and in our current experiments the structure is very small ($R \sim 1.7$ mm, $t \sim 0.03$ mm), we cannot ensure all of the samples have exactly the same structures and perfect cylindrical microtruss, so that there is different peak stress in Fig. 12. However from the experiment it is clearly shown the NMF liquid filler can effectively suppress the weakening of the load capacity after initial yielding which is exactly same as the previous FEM simulation results. Meanwhile the energy absorption capacity was improved by about 30%, from 0.28 J/cc to 0.37 J/cc. Here, the energy absorption improvement by NMF liquid filler in the experiments is much smaller than the FEM simulation results. This is because the studied microlattice structures are very small (diameter ~ 3.5 mm) and the air is hard to exclude during the injection of the NMF liquid. Therefore the energy absorption improvement is lowered by the presence of air.

4. Strain hardening effect

In Section 3, the constitutive relation of the parent material of the microtruss is elastic–perfectly plastic and in this section, the strain hardening effect of the parent material on the energy absorption for both NMF liquid filled microtruss and hollow microtruss is studied. The parent material of the microtruss is assigned bilinear stress–strain response such as aluminum alloy,

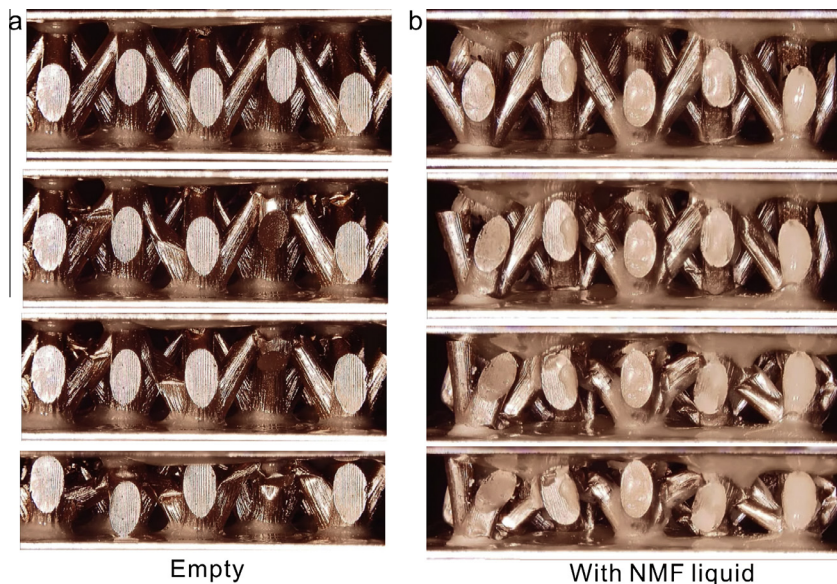


Fig. 11. The compressive deformation of 60° hollow microlattice (a) and NMF liquid filled microlattice (b).

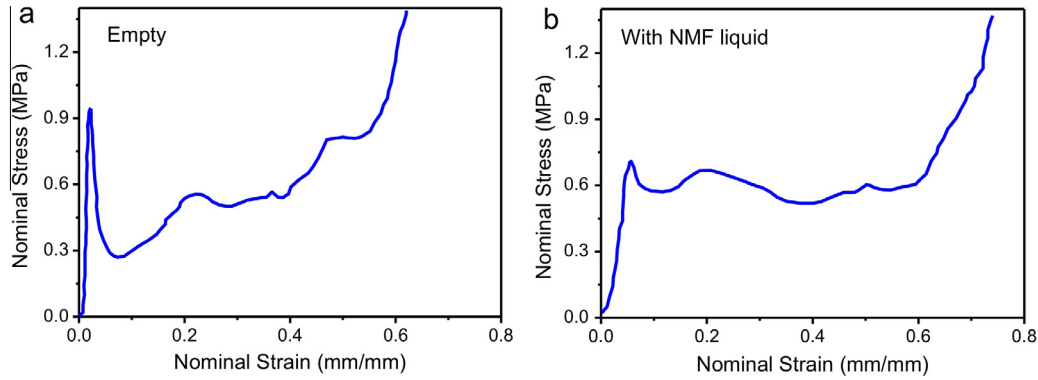


Fig. 12. Quasi-static compressive strain–stress curves of 60° hollow microlattice (a) and NMF liquid filled microlattice (b).

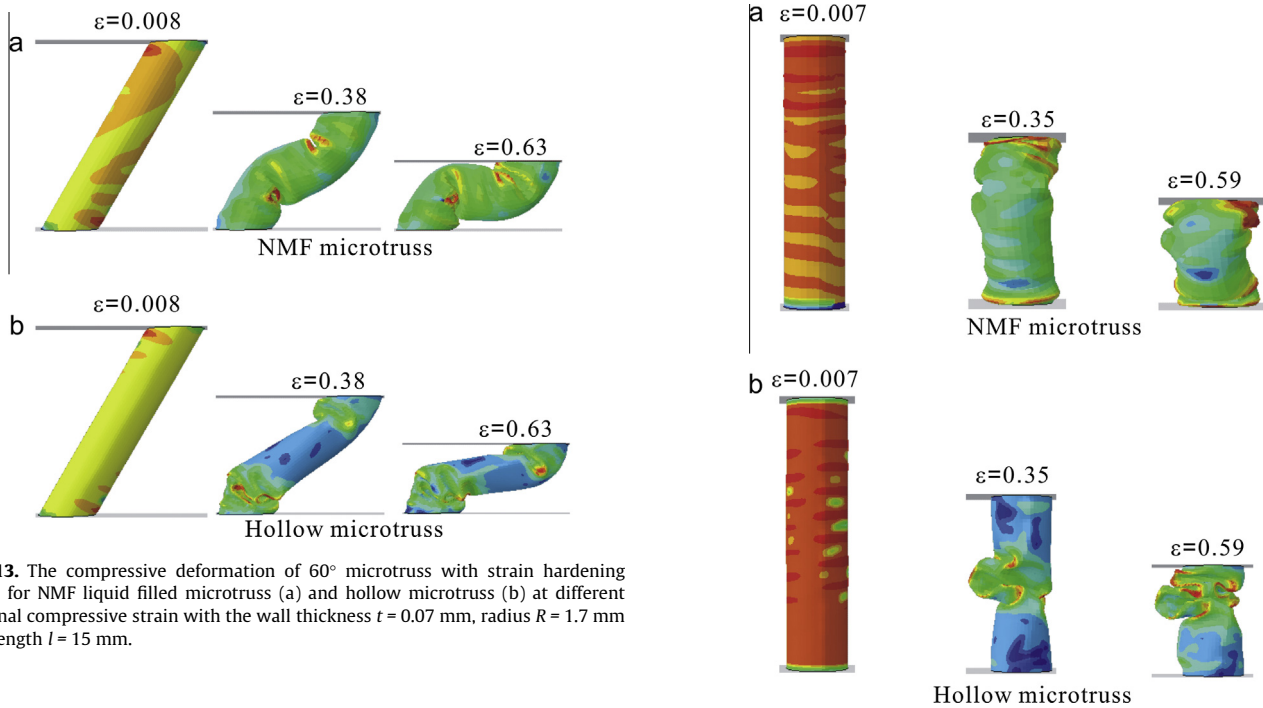


Fig. 13. The compressive deformation of 60° microtruss with strain hardening effect for NMF liquid filled microtruss (a) and hollow microtruss (b) at different nominal compressive strain with the wall thickness $t = 0.07$ mm, radius $R = 1.7$ mm and length $l = 15$ mm.

with moderate strain hardening (tangent modulus, $E_t/E = 0.01$) which is consisted with the previous work [9]. In order to compare the strain hardening effect on energy absorption, the density, Young's modulus and yield strength of the microtruss material are kept the same as the values listed in Section 3.

4.1. Compressive behavior

The compressive deformation of 60° microtruss with strain hardening effect is given in Fig. 13. The overall deformation is similar to that without strain hardening effect, for both NMF liquid filled microtruss and hollow microtruss, see Fig. 4. However, the stress distribution is different when strain hardening is taken into consideration. Here the contour plots represent the von Mises stress distribution in the microtruss. As the plastic strain is relative large at the wrinkles, the high stress region localizes at the wrinkles, and, thus, the further formation of wrinkles is suppressed. The number of wrinkles with strain hardening effect is less than the cases without strain hardening effect, and the wave length of the wrinkle is larger.

The compression of 90° microtruss with strain hardening effect for both NMF liquid filled microtruss and hollow microtruss is given in Fig. 14. The overall deformation is similar to the

Fig. 14. The compression of 90° microtruss with strain hardening effect of the microtruss for NMF liquid filled microtruss (a) and hollow microtruss (b) at different nominal compression strain with the wall thickness $t = 0.07$ mm, radius $R = 1.7$ mm and length $l = 15$ mm.

deformation of 90° microtruss without strain hardening effect as shown in Fig. 5. However, the wrinkles are suppressed by the strain hardening effect and the high stress region localizes near the wrinkles, which is somewhat similar to the condition of 60° microtruss with strain hardening.

In Fig. 15, the nominal stress–strain curves show that owing to the strain hardening effect, the stress slightly increases after initial buckling for both 60° and 90° microtrusses. This is different from the microtruss without strain hardening effect where the peak stress is the initial buckling stress. For the hollow microtruss, the stress quickly decreases to the same level of the hollow microtruss without strain hardening effect, and the energy absorption enhancement by strain hardening effect is negligible. On the other hand, with the strain hardening effect, the microtruss can support higher pressure to the NMF liquid inward and the optimized infiltration pressure of the NMF liquid is increased. The optimized infiltration pressure for 60° microtruss in Fig. 13 is about 18 MPa

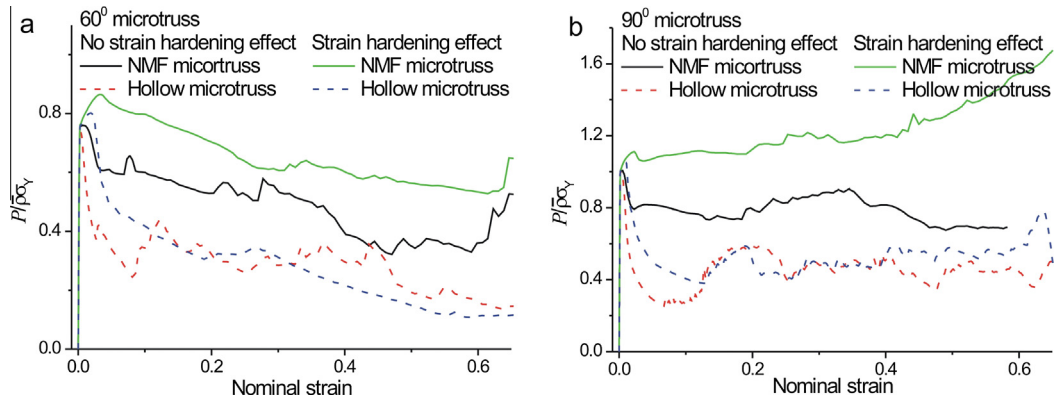


Fig. 15. The comparison of non-dimensional stress strain relation for NMF filled microtruss and hollow microtruss with and without strain hardening effect, for 60° microtruss (a) and 90° microtruss (b). The wall thickness of the microtruss is 0.07 mm, radius is 1.7 mm and length is 15 mm.

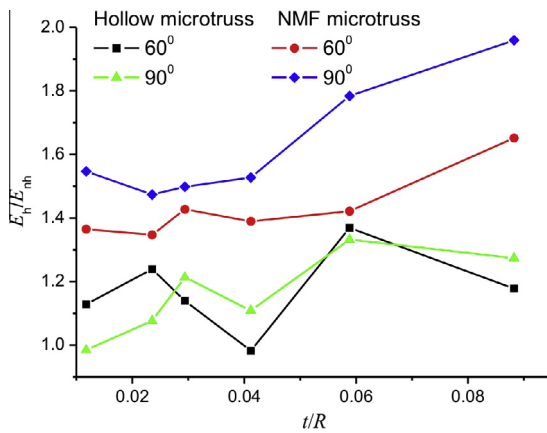


Fig. 16. The comparison of the energy absorption between microtruss with strain hardening effect and without strain hardening effect for 60° hollow microtruss (squares), 60° NMF liquid filled microtruss (circles), 90° hollow microtruss (triangles) and 90° NMF liquid filled microtruss (diamonds).

and for 90° microtruss in Fig. 14 is about 20 MPa which is two times the values without strain hardening effect studied in Section 3. Subsequently, the post buckling loads are significantly improved for both 60° and 90° microtruss. Therefore, the energy absorption is significantly improved for the NMF filled microtruss by counting for the strain hardening effect.

4.2. Energy absorption enhancement

The comparison of the energy absorption between microtruss with strain hardening and without strain hardening effect is given in Fig. 16. Here E_h is the energy absorption of microtruss with strain hardening effect and E_{nh} is its counterpart without strain hardening effect. The infiltration pressure of NMF liquid for microtruss with strain hardening effect and without strain hardening effect is optimized, respectively. The energy absorption enhancement of strain hardening effect for hollow microtruss is small and the energy absorption ratio of E_h/E_{nh} is between 1 and 1.3 for both 60° and 90° microtruss with different t/R , which is consistent with the stress–strain curves in Fig. 15.

By contrast, the strain hardening effect of microtruss can significantly help it to hold a larger infiltration pressure, thereby promoting energy absorption. The energy absorption enhancement by the strain hardening effect increases with t/R , for 60° microtruss the energy absorption ratio E_h/E_{nh} increases from 1.4 to 1.6 as t/R

increases from 0.01 to 0.09, while for 90° microtruss the energy absorption ratio is higher (from 1.6 to 2.0). Here E_{nh} is the energy absorption of NMF liquid filled microtruss of the same geometrical parameters without strain hardening effect. This is because for NMF liquid filled microtruss the beam-like bending is the overall deformation, and as t/R increases, the strain hardening effect contributes more to the energy absorption of beam-like bending. By introducing the strain hardening effect the energy absorption between NMF liquid filled microtruss and hollow microtruss $E_{nh,NMFtruss}/E_{nh,Hollow}$ is improved from 2 to 4.5 compared to the microtruss without strain hardening effect from 1.5 to 3 in the studying parameter.

5. Discussion

Although the energy absorption can be improved by NMF liquid filler, it is under the premise that no leaking takes place. If the microtruss fractures during compression, the NMF liquid will leak and the energy absorption enhancement by NMF liquid filler will be lost. The equivalent plastic strain of the microtruss during compression is given in Fig. 17. Here the equivalent plastic strain is defined as

$$\epsilon_{PEEQ} = \int_0^t \sqrt{\frac{2}{3}} \dot{\epsilon}_{pl} : \dot{\epsilon}_{pl} dt, \quad (27)$$

where $\dot{\epsilon}_{pl}$ is the increment of the plastic strain. For hollow microtruss without strain hardening effect the distribution of the equivalent plastic strain during compression is shown in Fig. 17(a). The high plastic strain localizes at the wrinkled region. For the hollow microtruss the energy absorption is contributed by the plastic deformation of shell, so the major energy absorption is at the regions of wrinkles, while the other part of the microtruss is not fully utilized. For the NMF filled microtruss, owing to the support of the NMF liquid, the distribution of equivalent plastic strain is more uniform, see Fig. 17(b). This is the additional energy absorption enhancement by shell of the microtruss depicted in Fig. 7. For the NMF liquid filled microtruss, there is also plastic strain localization at the wrinkles. As shown in Fig. 17(b), the maximum equivalent plastic strain is about 0.6 with the nominal compression strain of 0.63. At this large plastic strain, it may generate fracture in microtruss. Nevertheless, the energy absorption is still improved before the NMF liquid leaks. As the wrinkles can be suppressed by the strain hardening effect, for the NMF liquid filled microtruss with strain hardening effect, the equivalent plastic strain is more uniform and the maximum equivalent plastic strain is smaller (about 0.34 at the nominal strain of 0.63), see Fig. 17(c).

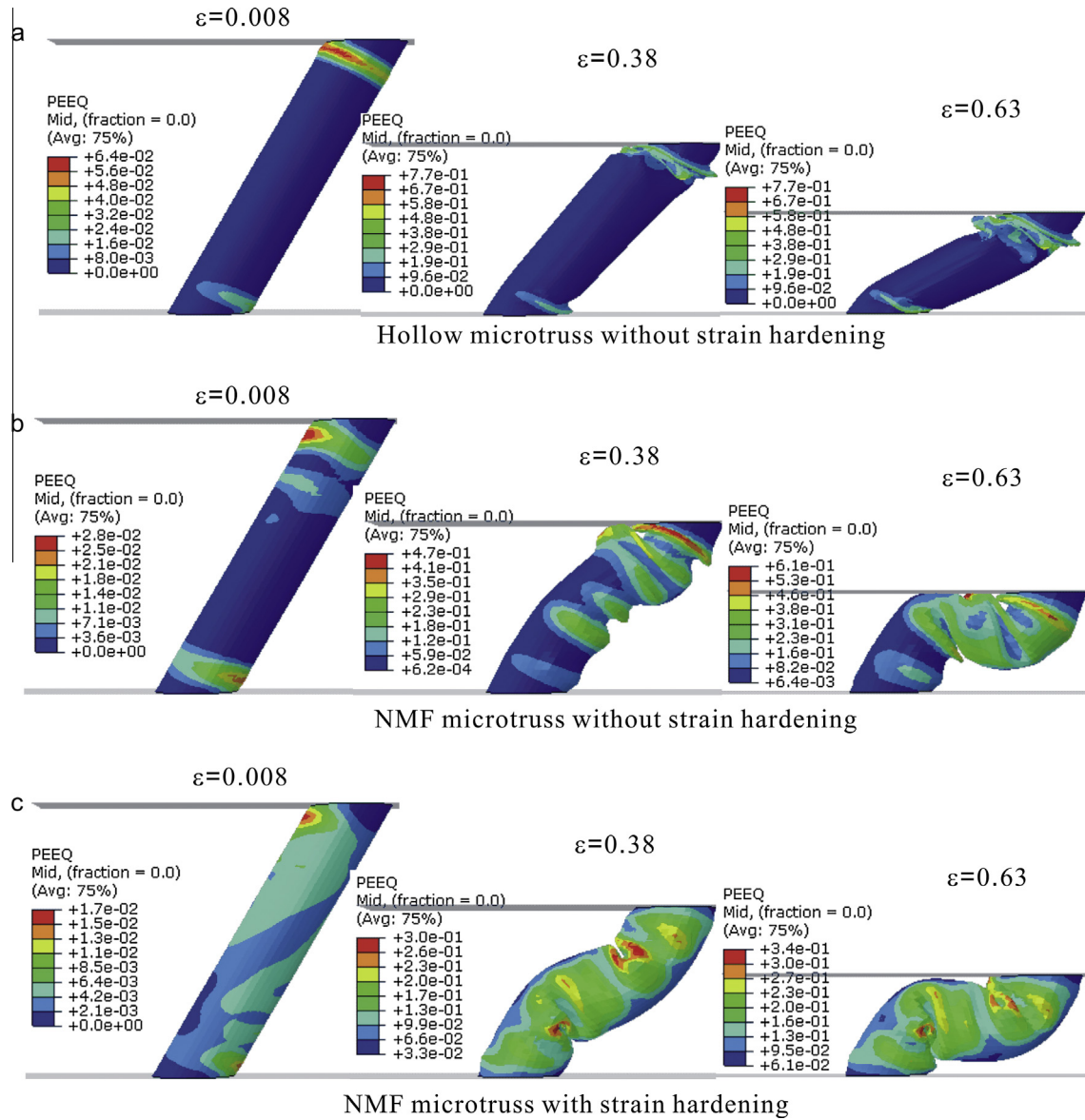


Fig. 17. The distribution of the equivalent plastic strain during compression for hollow microtruss without strain hardening effect (a), NMF liquid filled microtruss without strain hardening effect (b) and NMF liquid filled microtruss with strain hardening effect (c). The wall thickness of the microtruss is 0.07 mm, radius is 1.7 mm and length is 15 mm.

The leaking problem is a challenge for energy absorption enhancement by NMF liquid filler. In fact, we found that the leaking problem was not very serious in experiments. This may be caused by two reasons: the electroplate nickel employed in the experiments has limited strain hardening effect and the maximum equivalent plastic strain is smaller than that of FEM simulation (Fig. 17(b)); and the high plastic strain region is much localized at the wrinkles and the initial fracture may not propagate (that any fluid leakage may be slow). In order to avoid leaking, materials with high toughness such as polymer and composites, may be considered to construct the microtruss.

Furthermore, the hollow truss microlattice structures in the experiments are well-connected and the NMF liquid can flow through the microtruss members. This is especially useful to mitigate the ballistic impacting energy. Thanks to the fluidity of the NMF liquid, the pressure of the NMF liquid inside the whole microlattice is the same, which means that all of the NMF liquid can contribute to the energy absorption and protection of the

localized ballistic impacting. This is the spread effect of the NMF liquid which will be studied in future.

6. Conclusions

The energy absorption of hollow truss microlattice can be improved by NMF liquid filler. The compressive deformation map of hollow microtruss is given based on which the yielding criterion of NMF liquid filled microtruss is proposed. In order to fulfill the energy absorption capacity of NMF liquid, the infiltration pressure should be properly optimized. For 60° microtruss, the optimized infiltration pressure is $0.7\sigma Yt/R$ and for 90° microtruss it is $0.8\sigma Yt/R$. If the infiltration pressure of NMF liquid is too small, the potential of the energy absorption of NMF liquid is not fully utilized; on the other hand, if the infiltration pressure is too large, the infiltration process cannot occur and the NMF liquid becomes too rigid, so that the compressibility of the microtruss structure is weakened and the microtruss may be ruptured during

compression. The energy absorption enhancement by NMF liquid filler comes from two parts: one is the energy absorption by the NMF liquid and another is the energy absorption enhancement by the plastic deformation enhancement of the microtruss. The energy absorption enhancement by NMF liquid filler decreases as t/R increases. The ratio of energy absorption between NMF liquid filled microtruss and hollow microtruss ranges from 3 ($t/R = 0.01$) to about 1.5 ($t/R = 0.09$) for both 60° and 90° microtruss.

The energy absorption of NMF liquid filled microtruss can be further improved by the strain hardening effect of the materials of the microtruss. The enhancement by strain hardening effect increases as t/R increases, and the energy absorption can be improved about one fold for 90° microtruss with $t/R = 0.09$. Hence, by introducing the strain hardening effect the energy absorption between NMF liquid filled microtruss and hollow microtruss $E_{nh,NMFtruss}/E_{nh,Hollow}$ can achieve 4.5. The strain hardening effect can also reduce the plastic strain localization at the wrinkles of the microtruss during compression, which may help to suppress the leak of NMF liquid. This study reveals the energy absorption enhancement mechanism by NMF liquid filler, which may be helpful to design high energy absorption structures.

Acknowledgments

This investigation was sponsored by DARPA through the Soldier Protection Systems program managed by J. Goldwasser (contract no. W91CRB-11-C-0112). The views expressed are those of the author and do not reflect the official policy or position of the Department of Defense or the U.S. Government. YL acknowledges additional support from the National Natural Science Foundation of China (11302163 and 11321062) and XC acknowledges additional support from the National Natural Science Foundation of China (11172231 and 11372241), the World Class University program through the National Research Foundation of Korea (R32-2008-000-20042-0), and the National Science Foundation (CMMI-0643726). The authors would like to thank W.B. Carter for useful discussions and A. Sorensen and C. Ro (HRL Laboratories) for help with sample preparation and testing.

References

- [1] Aktay L, Toksoy A, Güden M. Quasi-static axial crushing of extruded polystyrene foam-filled thin-walled aluminum tubes: experimental and numerical analysis. *Mater Des* 2006;27:556–65.
- [2] Ashby M, Evans T, Fleck NA, Hutchinson JW, Wadley HNG, Gibson LJ. *Metal foams: a design guide*. Butterworth-Heinemann; 2000.
- [3] Ashby MF. The properties of foams and lattices. *Philos Trans Roy Soc A-Math Phys Eng Sci* 2006;364:15–30.
- [4] Banhart J. Manufacture, characterisation and application of cellular metals and metal foams. *Prog Mater Sci* 2001;46:559–632.
- [5] Chen W, Wierzbicki T. Relative merits of single-cell, multi-cell and foam-filled thin-walled structures in energy absorption. *Thin-Walled Struct* 2001;39:287–306.
- [6] Chen X, Surani FB, Kong X, Punyamurtula VK, Qiao Y. Energy absorption performance of steel tubes enhanced by a nanoporous material functionalized liquid. *Appl Phys Lett* 2006;89:241918.
- [7] D'Mello RJ, Waas AM. Synergistic energy absorption in the axial crush response of filled circular cell honeycombs. *Compos Struct* 2012;94:1669–76.
- [8] Davies GJ, Zhen S. Metallic foams – their production, properties and applications. *J Mater Sci* 1983;18:1899–911.
- [9] Evans AG, He MY, Deshpande VS, Hutchinson JW, Jacobsen AJ, Carter WB. Concepts for enhanced energy absorption using hollow micro-lattices. *Int J Impact Eng* 2010;37:947–59.
- [10] Evans AG, Hutchinson JW, Fleck NA, Ashby MF, Wadley HNG. The topological design of multifunctional cellular metals. *Prog Mater Sci* 2001;46:309–27.
- [11] Gibson LJ, Ashby MF. *Cellular solids: structure and properties*. New York: Cambridge University Press; 1997.
- [12] Han A, Punyamurtula VK, Kim T, Qiao Y. The upper limit of energy density of nanoporous materials functionalized liquid. *J Mater Eng Perform* 2008;17:326–9.
- [13] Hanssen AC, Langseth M, Hopperstad OS. Static and dynamic crushing of circular aluminium extrusions with aluminium foam filler. *Int J Impact Eng* 2000;24:475–507.
- [14] Jacobsen AJ, Barvosa-Carter W, Nutt S. Micro-scale truss structures formed from self-propagating photopolymer waveguides. *Adv Mater* 2007;19:3892–6.
- [15] Jacobsen AJ, Barvosa-Carter W, Nutt S. Micro-scale truss structures with three-fold and six-fold symmetry formed from self-propagating polymer waveguides. *Acta Mater* 2008;56:2540–8.
- [16] Kooistra GW, Deshpande VS, Wadley HNG. Compressive behavior of age hardenable tetrahedral lattice truss structures made from aluminium. *Acta Mater* 2004;52:4229–37.
- [17] Kwon YW, Cooke RE, Park C. Representative unit-cell models for open-cell metal foams with or without elastic filler. *Mater Sci Eng A: Struct Mater Prop Microstruct Process* 2003;343:63–70.
- [18] Liu L, Chen X, Lu W, Han A, Qiao Y. Infiltration of electrolytes in molecular-sized nanopores. *Phys Rev Lett* 2009;102:184501.
- [19] Liu Y, Schaedler TA, Jacobsen AJ, Chen X. Quasi-static energy absorption of hollow microtruss structures. *Composites Part B*, submitted for publication.
- [20] Maloney KJ, Fink KD, Schaedler TA, Kolodziejska JA, Jacobsen AJ, Roper CS. Multifunctional heat exchangers derived from three-dimensional micro-lattice structures. *Int J Heat Mass Transf* 2012;55:2486–93.
- [21] Qiao Y, Liu L, Chen X. Pressurized liquid in nanopores: a modified laplace-young equation. *Nano Lett* 2009;9:984–8.
- [22] Qin Q, Wang T. Low-velocity impact response of fully clamped metal foam core sandwich beam incorporating local denting effect. *Compos Struct* 2013;96:346–56.
- [23] Queheillalt DT, Wadley HNG. Cellular metal lattices with hollow trusses. *Acta Mater* 2005;53:303–13.
- [24] Schaedler TA, Jacobsen AJ, Torrents A, Sorensen AE, Lian J, Greer JR, et al. Ultralight metallic microlattices. *Science* 2011;334:962–5.
- [25] Surani FB, Kong XG, Panchal DB, Qiao Y. Energy absorption of a nanoporous system subjected to dynamic loadings. *Appl Phys Lett* 2005;87:163111.
- [26] Sypeck DJ, Wadley HNG. Multifunctional microtruss laminates: textile synthesis and properties. *J Mater Res* 2001;16:890–7.
- [27] Tilbrook MT, Deshpande VS, Fleck NA. The impulsive response of sandwich beams: analytical and numerical investigation of regimes of behaviour. *J Mech Phys Solids* 2006;54:2242–80.
- [28] Timoshenko SP, Gere JM. *Theory of elastic stability*. McGRAW-HILL INTERNATIONAL BOOK COMPANY; 1963.
- [29] Valdevit L, Wei Z, Mercer C, Zok FW, Evans AG. Structural performance of near-optimal sandwich panels with corrugated cores. *Int J Solids Struct* 2006;43:4888–905.
- [30] Vesenjak M, Krstulovic-Opara L, Ren Z, Oechsner A, Domazet Z. Experimental study of open-cell cellular structures with elastic filler material. *Exp Mech* 2009;49:501–9.
- [31] Wadley HNG, Fleck NA, Evans AG. Fabrication and structural performance of periodic cellular metal sandwich structures. *Compos Sci Technol* 2003;63:2331–43.
- [32] Xu B, Qiao Y, Chen X. Mitigating impact/blast energy via a novel nanofluidic energy capture mechanism. *J Mech Phys Solids* 2014;62:194–208.
- [33] Zhao J, Culligan PJ, Germaine JT, Chen X. Experimental study on energy dissipation of electrolytes in nanopores. *Langmuir* 2009;25:12687–96.